Alignment control of clay and its effect on properties of polymer nanocomposites

Morimune-Moriya, Seira

Kotera, Masaru

Nishino, Takashi

(Citation)
Polymer,256:125202

(Issue Date)
2022-09-21

(Resource Type)
journal article

(Version)
Accepted Manuscript

Alignment Control of Clay and Its Effect on Properties of Polymer Nanocomposites

Seira Morimune-Moriya[a]*, *Masaru Kotera*[b], *Takashi Nishino*[b]

[a] *Department of Applied Chemistry, College of Engineering, Chubu University, Matsumoto, Kasugai 487-8501, Japan*

[b]*Department of Chemical Science and Engineering, Graduate School of Engineering, Kobe University, Rokko, Nada, Kobe 657-8501, Japan*

Tel: 81-568-51-9423, Fax: 81-568-51-1499, E-mail: seiram@isc.chubu.ac.jp

ABSTRACT.

Polymer nanocomposites are well known to show high performances by the addition of a small amount of nanofiller. However, the brittleness has often been reported as a general issue of the nanocomposites. In this study, we revealed the excellent toughening effect of poly (vinyl alcohol) (PVA)/montmorillonite (MMT) nanocomposites by controlling the alignment of MMT by drawing. The PVA/MMT nanocomposites with 5 wt% MMT loading was prepared and then drawn by uniaxial drawing, roll drawing and simultaneous-biaxial drawing. The drawn nanocomposites, where MMT was highly aligned parallel to the film surface, showed excellent enhancement in the mechanical properties and barrier properties. It is noteworthy that not only the Young's modulus and the tensile strength, but also the elongation at break and the toughness remarkably increased for the drawn nanocomposites. For example, the simultaneously-biaxially-drawn nanocomposite showed the toughness of 17 times higher than that of the as-cast nanocomposite. Furthermore, the swelling ratio was comparable to that of surface fluorinated PVA film.

Keywords: Polymer nanocomposites; Orientation; Stress transfer

1. Introduction

Clay reinforced nylon 6 nanocomposite by Toyota Central R&D Labs., Inc. was the first major success with polymer nanocomposites.[1-6] Since then, many researchers have actively engaged on polymer nanocomposites all over the world. Nanocomposites, in which a small amount of nanofillers are incorporated, show remarkable improvement in materials' properties compared with those of virgin polymers or conventional micro-fillers incorporated composites. The works on nanocomposites have spread to a wide variety of polymer matrices as well as to a various nano-fillers, such as nano-fibers and nanocarbons.[7–15] Clay has often been used as one of nano-fillers to improve not only mechanical properties and thermal properties, but also fire retardancy and barrier properties of polymer materials by taking advantage of its sheet-like geometry with high aspect ratio.[16-20]

Montmorillonite (MMT) is a clay which has been extensively used as a filler for polymer nanocomposites. A single layer is composed of silicon tetrahedral – aluminum octahedral – silicon tetrahedral sheet stacking with the thickness of only 1 nm and it possesses very high aspect ratio in the range of 10–1000.[21] Due to its hydrophilic nature, hydrophobic monomers and/or polymers cannot be intercalated into the layers, or the layers cannot be exfoliated individually in polymer matrices. As for the nylon6/clay nanocomposites shown above, MMT was organically modified with cationic surfactant, such as alkyl ammonium cations, to improve the dispersibility in the polymer matrices. [1-6] Similarly, organified MMT has often been incorporated into polymers, including

polyolefins, polyester, epoxy and so on. [6] On the other hand, MMT is known to highly swell in water and form stable aqueous suspensions with monolayers.[22] It has been reported to be well dispersed as fully exfoliated monolayers in the hydrophilic polymers, such as poly (vinyl alcohol) (PVA)[22–25] and poly (ethylene oxide)[26,27] and cellulose[28,29] without any organic modification.

In our previous study, we revealed the stress transfer system in the PVA/MMT nanocomposites by the 'X-ray diffraction method'.[30] The stress on the PVA/MMT nanocomposites was shown to be transferred quite effectively to MMT. As a result, the Young's modulus and the tensile strength significantly increased by the incorporation of even small amount of MMT. On the other hand, as a common issue for polymer nanocomposites, the elongation at break and toughness decreased due to the brittleness of rigid fillers. It is well known that the dispersibility of fillers and the interfacial interaction between filler and polymer matrix are important factors to achieve the high performance of the nanocomposites. In this regard, MMT was highly exfoliated and highly dispersed at nano-level in PVA, in addition, the strong interfacial interactions of hydrogen bonds were formed between MMT and PVA.

In this study, we focus on the alignment of MMT platelets and the orientation of PVA crystallites. It has been reported that the drawing of polymer nanocomposites with high-aspect-ratio-filler largely affected the orientation of polymer crystallites and the alignment of the fillers, resulted in the remarkable changes in the structures and the properties of the nanocomposites, such as crystallinity, mechanical properties and barrier properties.[31-35] Here in, we controlled the alignment of MMT

platelets and the orientation of PVA crystallites by three kind of drawing method, uniaxial drawing, biaxial drawing and roll drawing. The effect of the drawing on the structure of the nanocomposites were examined in detail, and the effect of the alignment of MMT on mechanical properties and barrier properties of the nanocomposites were investigated.

2. Experimental Section

2.1. Materials

PVA was supplied from Nippon Synthetic Chemical Industry Co., Ltd. with its commercial name "Gohsenol NH-18"; the degree of polymerization was 1,800 and the degree of saponification was more than 99%. MMT was supplied by Kunimine industries, Co. Ltd. with its' commercial name "Kunipia-G". All the materials were used as received.

2.2. Sample preparation

MMT was stirred in ion-exchanged water for 1 day, and then PVA powder was added to the MMT aqueous suspension and dissolved at 90 ºC under stirring. The MMT content was controlled to be 5 wt%. The PVA/MMT aqueous suspension was casted into a petri dish. After dried at room temperature, the nanocomposite was taken out and was dried at 40 ºC for 48 h in vacuum. The thickness of the resulted nanocomposite was ca. 250 μm. The as-cast (AC) nanocomposite was drawn by uniaxial drawing (UD), roll drawing (RD) and simultaneous biaxial drawing (SBD). The conditions of the drawing processes were summarized in Table 1.

Table 1 Drawing conditions.

Drawing method	Temperature	Speed	Original length
	ºC	mm/min	mm
Uniaxial	120	90	90
Roll	120	90	90
Simultaneous biaxial	140	30	30

2.3. Characterization

X-ray diffraction was carried out with an X-ray diffractometer (Rigaku, RINT2100). The specimen was irradiated by Ni-filtered CuKα radiation beam (wavelength=1.5418 Å) operated at 40 kV/20 mA. The scanning speed was 1.0 °/min and the $2\theta/\theta$ scan data were collected at 0.02 ° intervals. X-ray diffraction images were taken using a synchrotron radiation at the beam line of BL-24XU of SPring8 at the Hyogo Beamline. The X-ray beam (wavelength=1.2399 Å) was irradiated in through, edge and end direction of the specimen. The beam size was 250 μm and the radiation time was 30 min.

The cross section of the nanocomposite was observed using a field emission scanning electron microscope (FE-SEM) (JEOL, JSM-6700F) at an accelerating voltage of 10 kV. Pt/Pd was deposited on the sample surface prior to the observation.

The tensile properties were evaluated by tensile test using a tensile tester (Shimadzu Co., Autograph AGS-1kND). The initial length was 20 mm and a cross head speed of 2 mm/min was employed. The number of tested specimens was more than ten. The toughness (K) was determined as the area surrounded by the stress–strain curve. It was calculated using the following equation:

$$K=\int_{\varepsilon=0}^{\varepsilon=\varepsilon_{max}} \sigma \cdot d\varepsilon \quad /d \quad (J/g) \qquad (1)$$

where, σ is stress (Pa), ε is strain (%) and d is density (m^3/g). Dynamic mechanical analyses were performed by a dynamic mechanical analyzer (ITK Co., Ltd., DVA-220S), under nitrogen flow. A heating rate of 6 °C /min was employed with a frequency of 10 Hz. The same analyzer was used to measure the humidity dependence of the storage modulus. The relative humidity (RH) was changed from 15%RH to 90%RH at a rate of 1%RH/min in the air atmosphere at 60 ºC.

Swelling ratio was determined by immersing the specimen in distilled water at 30 ºC and was defined as the weight gain of the specimen as follows:

$$\text{Swelling ratio}=W/W_0 \qquad (2)$$

where, W_0 and W is the weight of the specimen before and after swelling, respectively. Water vapor permeation behavior was measured based on ASTM method of 96B. The specimen was placed over the top of a cup filled with distilled water at 30 ºC with the relative humidity of 30%RH.

3. Results and Discussion

3.1. Structure

Figure 1 (a) shows the SEM images of MMT from cross section. The layered structure of MMT was observed. The X-ray diffraction also confirmed the existence of the MMT interlayer. Figure 1 (b) shows the X-ray diffraction profiles of MMT, PVA/MMT nanocomposite and AC PVA film. On the profile of MMT, the 001 and 005 reflections were clearly observed at $2\theta = 7^\circ$ and 28°, respectively.[36] The weak diffraction peak of the 060 reflection was appeared at 2θ of 62°. As shown in the schematic

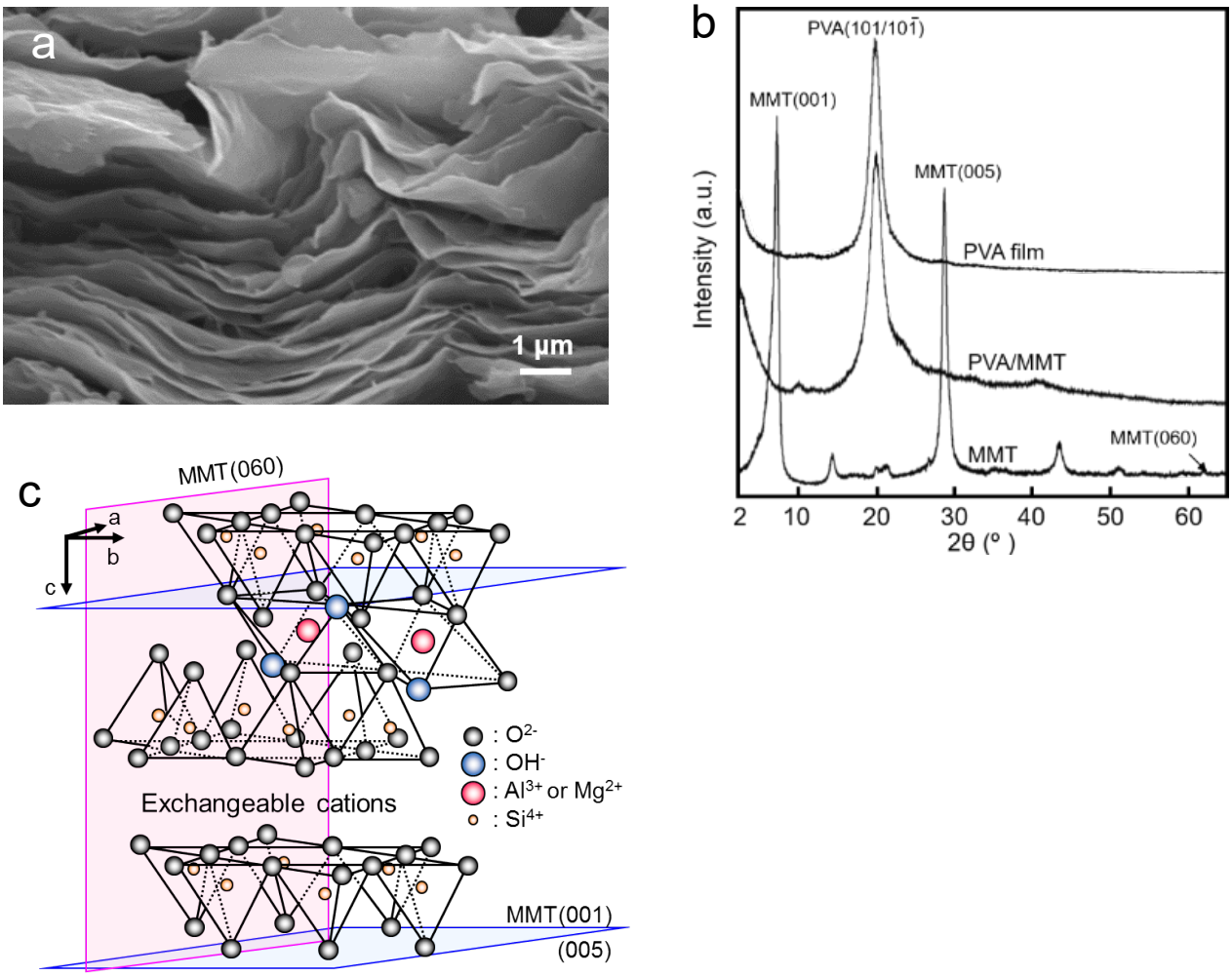

Figure 1 (a) SEM image of MMT from cross section; (b) X-ray diffraction profiles of AC PVA film, PVA/MMT nanocomposite and MMT; (c) schematic model of MMT crystal.

model of MMT crystal in Figure 1 (c), the 001 and 005 reflections derived from MMT interlayer while the 060 reflection was perpendicular to the interlayer (Figure 1 (c)). In the profile of PVA/MMT nanocomposite, 101/10$\bar{1}$ reflection of PVA clearly appeared at 2θ of 20 °. The 001 and 005 reflections of MMT was not observed in the profile of the nanocomposite, indicating that the silicate layers of MMT were intercalated or exfoliated and nano-dispersed in PVA matrix.[25] The crystallinity of the

PVA film and that of the PVA/MMT nanocomposite were found to be 28% and 33%, respectively.

Since MMT was highly dispersed in PVA, MMT served as a crystallization nucleus for PVA.

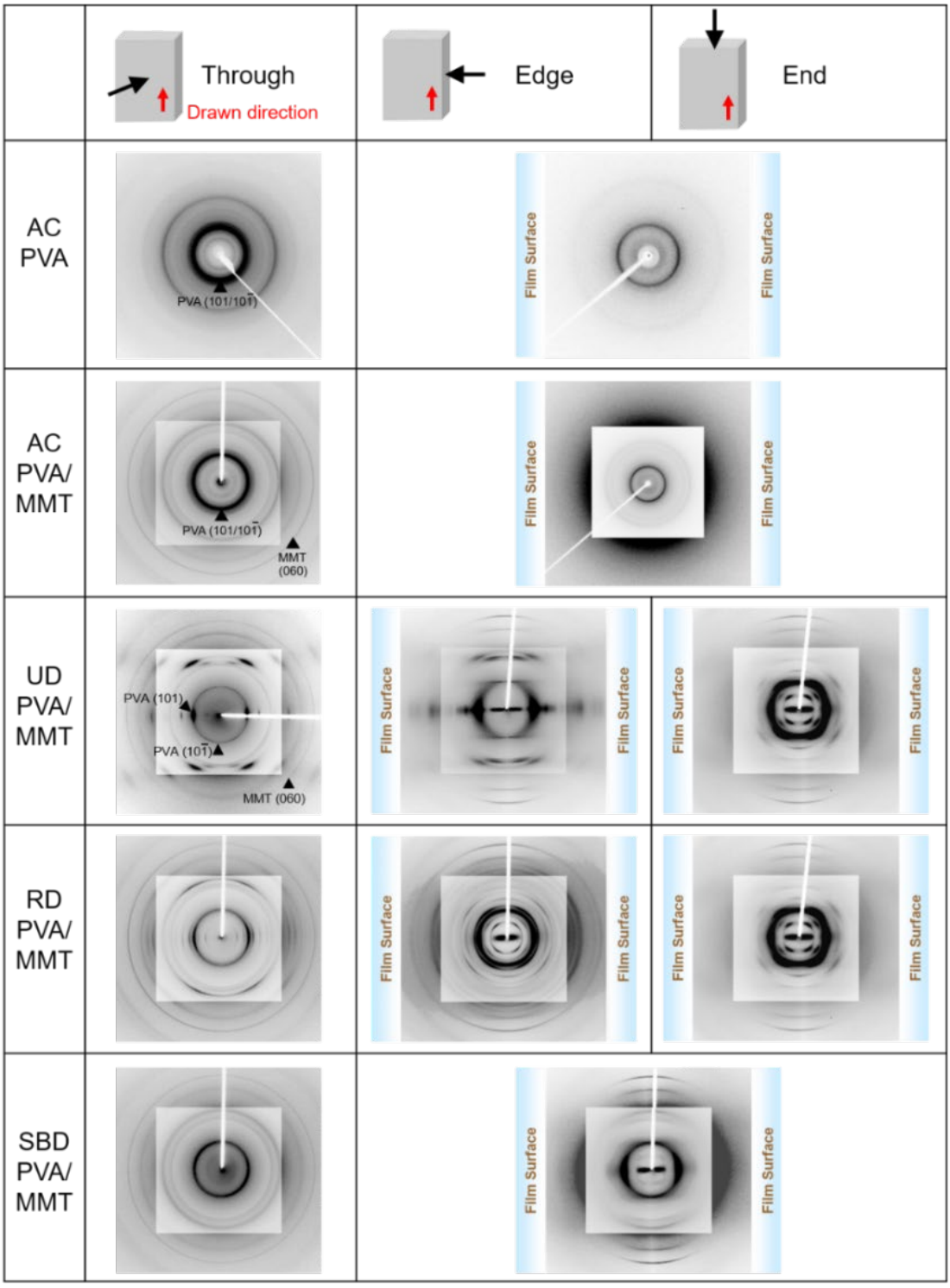

Figure 2 X-ray diffraction images of AC PVA film and AC, UD, RD and SBD PVA/MMT nanocomposite with an X-ray beam irradiated from through, edge, end and edge/end direction (draw ratio = 3). The contrast was controlled for better view.

Figure 2 shows the X-ray diffraction images of the AC PVA film and the AC, UD, RD and SBD nanocomposites. The X-ray beam irradiated from through, edge and end directions. In order to observe the weak reflections at higher diffraction angle, the images of the nanocomposites were piled up with two different contrasts. In the images of AC samples, the diffractions from PVA and MMT appeared as homogeneous Debye-Scherrer rings in both through and edge/end direction. The homogeneous Debye-Scherrer rings attributed to the random orientation of PVA crystallites and the random alignment of MMT platelets. Similar to the AC samples, the diffractions from MMT appeared as homogeneous Debye-Scherrer rings in the through direction of all the drawn nanocomposites, showing the random alignment of MMT. The typical fiber diffraction pattern was observed for the UD nanocomposites in the through direction. The $101/10\bar{1}$ reflection of PVA was clearly shown as the equatorial arc pattern. This pattern indicates that PVA crystallites were oriented to the drawn direction.[32] The diffraction pattern of the RD nanocomposites also indicated the orientation of PVA crystallites, while the degree of orientation was much lower than that of the UD nanocomposites. Only the SBD nanocomposites showed random orientation of PVA in the through direction among the drawn nanocomposites. Since the tensile stress was applied biaxially simultaneously at the same rate, polymer chains as well as MMT platelets distributed homogeneously in random pattern.

The 060 reflection of MMT in the edge/end direction were focused on the meridional direction for all the drawn nanocomposites. Since the (060) plane is perpendicular to the layer as shown in Figure 1 (c), the alignment of MMT platelets were revealed to be parallel to the film surface. Regarding the

orientation of PVA, the diffraction patterns of the drawn nanocomposites indicated that the PVA molecular chains took a planar zig zag conformation in the drawn nanocomposites as reported in previous literature. [37-40]

Figure 3 shows the SEM image of the cross section of the (a) AC and (b) SBD PVA/MMT nanocomposites. MMT were observed as bright portions. The 2D fast Fourier transformed (2D-FFT) image was superimposed in the corner of Figure 3. The random alignment of MMT platelets were observed in the AC nanocomposites, while it was highly aligned parallel to the film surface in the SBD nanocomposites. These results were in good agreement with the results of the X-ray diffraction images shown above. Furthermore, in comparison to the AC nanocomposite, the dispersibility of MMT in the drawn nanocomposite was revealed to be higher than that in the AC nanocomposites. It was suggested that the degree of exfoliation was enhanced by the shearing stress applied by the drawing.

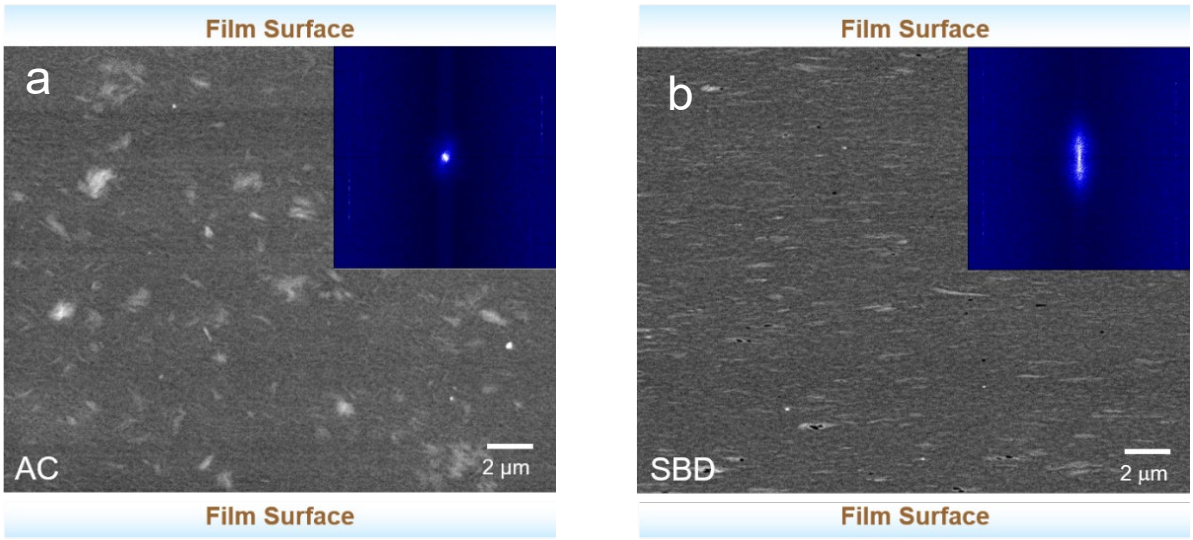

Figure 3 SEM image of the cross section of (a) AC and (b) SBD PVA/MMT nanocomposite. The 2D fast Fourier transformed image of the SEM image was superimposed on the upper right corner of the figure.

3.2. Mechanical properties

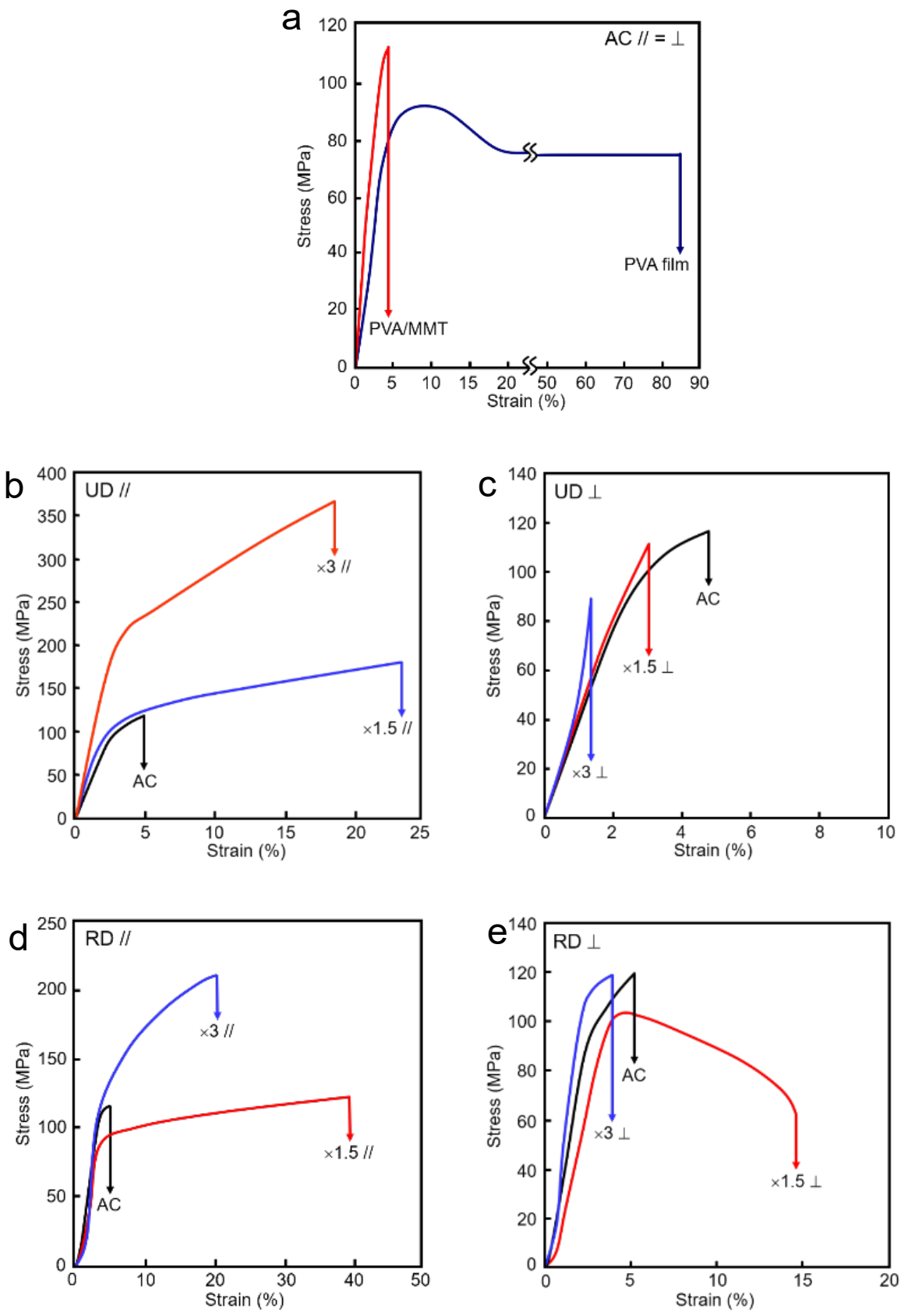

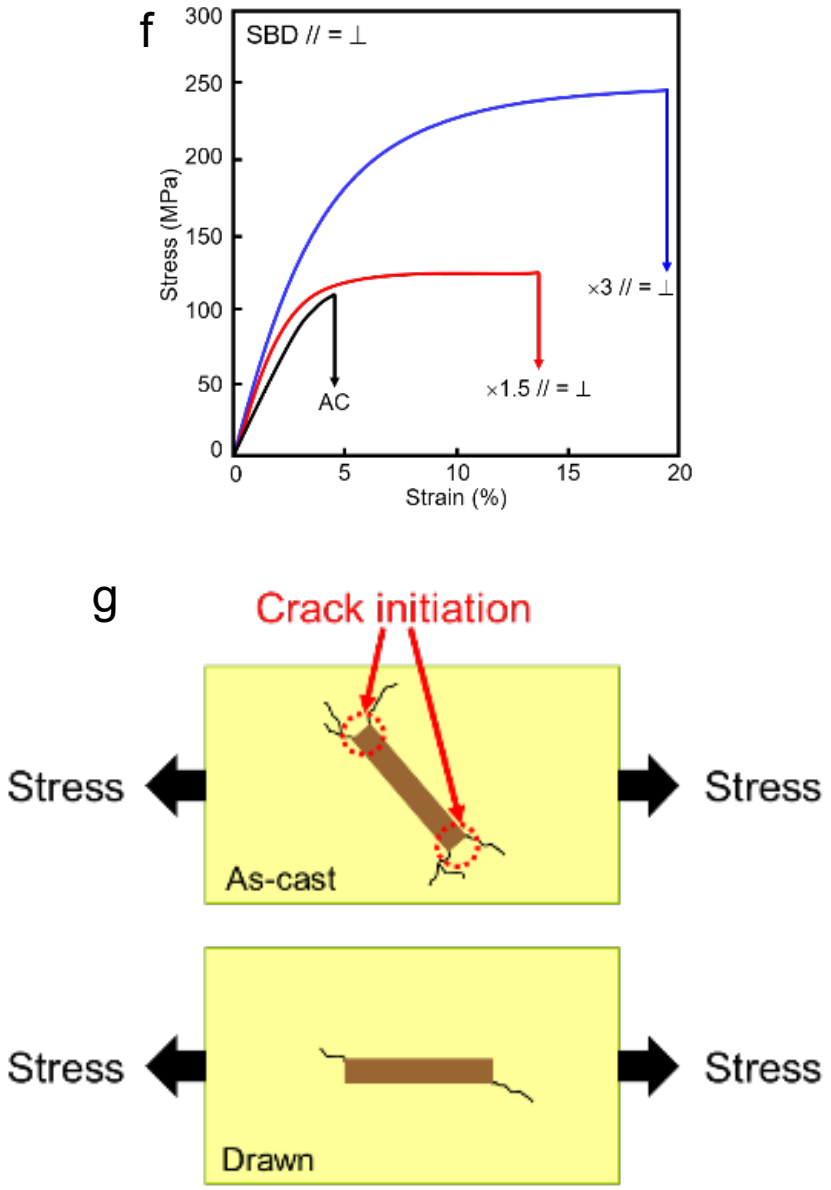

Figure 4. Stress-strain curves of (a) AC (//=⊥), (b) UD (//), (c) UD (⊥), (d) RD (//), (e) RD (⊥), and (f) SBD (//=⊥) PVA/MMT nanocomposites. The direction of the applied stress was parallel (//), perpendicular (⊥) and parallel=perpendicular (//=⊥) to the drawing direction. For comparison, the curve for the AC PVA/MMT nanocomposite was superimposed in each figure; (g) Schematic illustrations of failure mode in AC and drawn PVA/MMT nanocomposite during tensile test.

Table 2 Mechanical properties of AC PVA film and AC and drawn PVA/MMT nanocomposite.

			Young's modulus	*Tensile strength*	*Elongation at break*	*Toughness*
			GPa	MPa	%	J/g
PVA	AC // =⊥	-	3.2	92	81	47
PVA/MMT	AC // = ⊥	-	4.2	110	4.1	1.7
	UD //	×1.5	4.3	124	23	15
		×3	6.2	214	18	21
	UD ⊥	×1.5	3.4	103	3.1	0.9
		×3	4.6	119	1.4	0.3
	RD //	×1.5	6.0	184	39	21
		×3	8.2	366	20	16
	RD ⊥	×1.5	4.2	111	14	4.8
		×3	4.0	89	3.9	1.3
	SBD // = ⊥	×1.5	5.3	122	14	9.7
		×3	8.3	245	19	28

Figure 4 (a) shows the stress–strain curves of the AC PVA film and AC nanocomposite. The AC PVA film showed a typical curve for the conventional crystalline polymer, that was, the maximum in the curve was followed by yielding. On the other hand, a sharp increase in the stress followed by a brittle fracture was observed in the curve of the AC nanocomposite. The Young's modulus, tensile strength, elongation at break and the toughness obtained from these stress-strain curves were

summarized in Table 2. The Young's modulus and the tensile strength of the nanocomposite increased by 31% and 20%, respectively. The PVA/MMT nanocomposite was effectively reinforced by strong interactions, such as hydrogen bonding, at the interface between MMT platelets and the PVA matrix.[25,41] These favorable interactions and the high dispersibility of MMT in PVA brought the excellent stress transfer, resulted in the high mechanical properties of the nanocomposite. However, the toughness of the nanocomposite drastically decreased compared with that of the AC PVA film.

So far, rigid fillers such as nanocarbons have often been incorporated in polymer matrices, expecting the strong reinforcement effect. The enhancement in the Young's modulus and the tensile strength has often been reported, however, rigid fillers have brought the brittleness and have resulted in abrupt reduction of the toughness. It is well known that the agglomerates of fillers or poor interfacial interactions can cause crack initiation on polymer composites. Though many efforts have been made to improve the dispersibility of fillers in polymer matrices as well as the interfacial interactions, it is rare to obtain the increase in the elongation at break and the toughness by the incorporation of rigid fillers.

Figure 4 (b)-(f) show the stress–strain curves of the drawn PVA/MMT nanocomposites. The stress was applied to the direction parallel (//) or perpendicular (⊥) to the orientation. The elongation at break tend to decreased for the perpendicular direction of the UD and the RD nanocomposites. Since the PVA molecular chains uniaxially oriented parallel to the drawn direction, the physical interactions brought by the entanglements of polymer chains were reduced for the perpendicular direction of the

UD and the RD nanocomposites. Therefore, dissociation of the interaction between the polymer chains could easily occur so that the toughness drastically decreased. Only the RD nanocomposites with the drawn ratio of 1.5 showed the large increase in the elongation at break. Due to the low orientation degree of PVA as shown above, it was assumed that the favorable rate of entanglement of the PVA molecular chains were remained in the RD nanocomposites at the drawn ratio of 1.5. Therefore, the stress transfer was successfully achieved together with the toughening effect of the aligned MMT explained below.

The stress-strain curves for the parallel direction of the drawn nanocomposites showed quite unique behavior. It is noteworthy that not only the Young's modulus and the tensile strength but also the elongation at break were increased by drawing. As a result, the drawn nanocomposites showed strong enhancement in the toughness. The SBD nanocomposites with the drawn ratio of 3 showed the highest toughness, that was 17 times higher than that of the AC nanocomposites.

In the AC PVA/MMT nanocomposite, where MMT platelets were randomly aligned, the anisotropic morphology of MMT platelets caused the sharp defects due to the high stress concentration at the edge. The failure mode of the nanocomposite was schematically illustrated in Figure 4 (g). The defects led to early and low-energy fracture of the nanocomposite, which brought the drastic decrease in the elongation at break and the toughness.[42,43] As shown above, MMT platelets aligned parallel to the film surface in the drawn nanocomposites. Therefore, the interfacial area which was perpendicular to the applied stress, was decreased by drawing. Accordingly, the stress concentration at the platelet edge,

which caused the crack initiation, decreased in the drawn nanocomposites. In addition, the parallel orientation of the MMT platelets provide an effective barrier for the dominant deformation which caused by the cracks advancing perpendicular to the film surface.[44] The formation of the micro-cracks between the aligned MMT platelets and the 'damage zone'[45,46] at the interface partially absorb the stored strain energy and dissipating the deformation energy.[47,48]

Another toughening mechanism can be explained by the sacrificial bonds (hydrogen bonds and van der Waals interaction) and the stretching of hidden length at the interface.[49,50] Under the stress applied to the PVA/MMT nanocomposites, cleavage of the sacrificial bonds occurs, at the same time, the hidden length of PVA was released at the interface. Therefore, favorable slippage of parallel-aligned MMT enhanced the energy dissipation in the nanocomposites, resulted in the highly balanced mechanical properties.

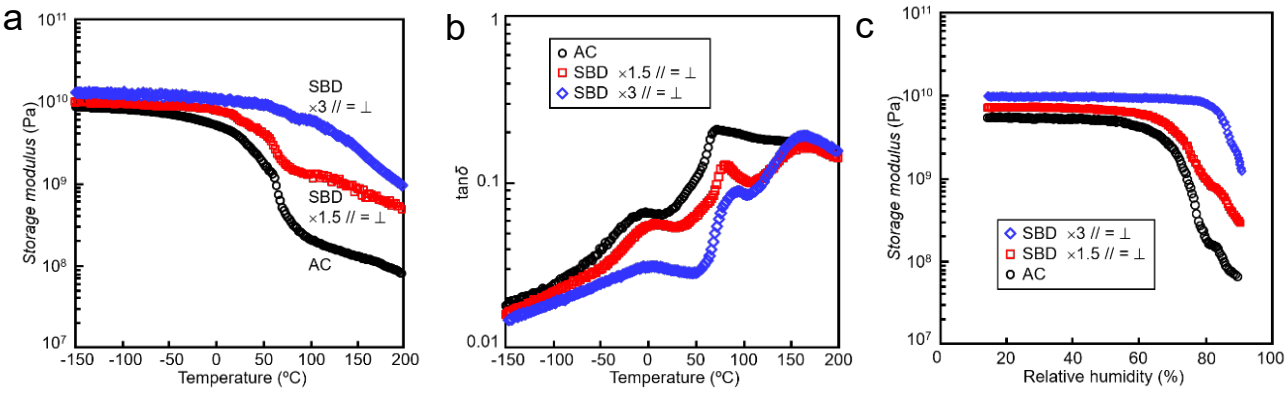

Figure 5. Temperature dependence of (a) storage modulus and (b) tanδ of AC and SBD PVA/MMT nanocomposite; (c) Relative humidity dependence of storage modulus of AC and SBD PVA/MMT nanocomposite at 60 ˚C.

Figure 5 shows temperature dependences of (a) the storage modulus and (b) the mechanical tanδ of the AC and the SBD nanocomposites. The SBD nanocomposite drawn by 3 times showed 10^9 Pa order of storage modulus even in high temperature up to 200 ˚C, while it was drastically decreased at around 60 ˚C for the AC nanocomposites. The intensities of mechanical tanδ of the SBD nanocomposites were lower than that of the AC nanocomposite. In addition, the main dispersion in the tanδ, the so-called α_a dispersion (approximately 61 ˚C), and the β dispersion (approximately -5 ˚C) was shifted to higher temperature by drawing. It was revealed that the aligned MMT platelets suppressed the molecular motion of PVA in the amorphous region, thus the glass transition temperature of the PVA matrix increased.

The relative humidity dependence of the storage modulus of the AC and the SBD nanocomposites were shown in Figure 5 (c). Compared to the AC nanocomposites, the SBD nanocomposites exhibited the higher storage modulus in the wide range of humidity (15%RH – 90%RH at 60 ºC) even at more than 80%RH at the drawn ratio of 3, suggesting that the high barrier properties against water was exploited to the nanocomposites by the highly aligned MMT.

3.3. Barrier properties

Figure 6 (a) shows the swelling ratio of the AC PVA film, PVA/MMT nanocomposite and the SBD nanocomposite in distilled water at 30 ˚C. The swelling ratio of the surface fluorinated PVA film reported by Nishino *et al.*[51] was inserted as the dotted line. The AC PVA film showed high swelling

due to its water solubility. The swelling ratio was effectively suppressed by the incorporation of MMT and by drawing. In the initial stage, the swelling ratio of the SBD nanocomposite was higher than that of surface fluorinated PVA film. The fluorinated surface strongly prevented the intrusion of water molecules due to its very low surface energy. However, after 150 min, the SBD nanocomposite suppressed the swelling ratio by 60% compared with that of PVA film and it was almost the same with the surface fluorinated PVA film, suggesting that the penetration pathway of water molecules was largely hampered by the highly aligned MMT platelets together with the strongly restricted molecular motion of PVA, resulting in the excellent barrier properties.

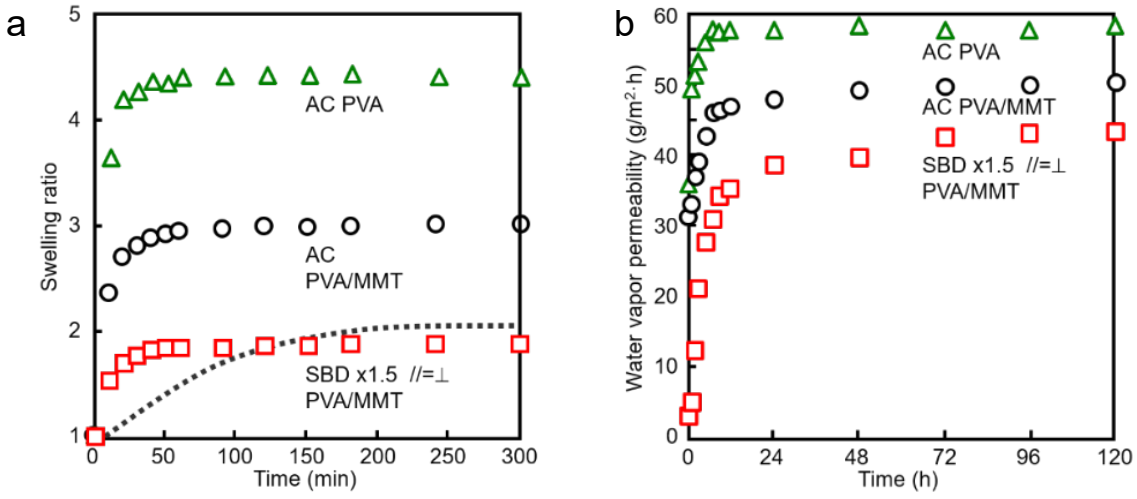

Figure 6. (a) Swelling ratio of AC and SBD PVA/MMT nanocomposite; (b) Water vapor permeability of AC and SBD PVA/MMT nanocomposite. The swelling ratio of the surface fluorinated PVA film [51] was shown as the dotted line. The surface fluorinated PVA was prepared by chemical modification of PVA film surface with fluorinated silane coupling agent.

Figure 6 (b) shows the water vapor permeation behavior of the SBD nanocomposite at 30 ˚C with that of AC PVA film and nanocomposite for comparison. As well as the swelling ratio, the water vapor permeability was successfully suppressed by the drawing in addition to the incorporation of MMT and the drawing.[52,53] The final permeability of the SBD nanocomposite was 15% lower than that of the AC nanocomposites, confirming the strong barrier effect of the highly aligned MMT platelets in the drawn nanocomposites.

4. Conclusions

The alignment control of MMT was conducted by drawing the PVA/MMT nanocomposites by UD, RD and SBD. The MMT platelets aligned parallel to the film surface by the drawing. In addition, the PVA crystallites in UD and RD nanocomposites were oriented parallel to the drawn direction. As a result, not only the Young's modulus and the tensile strength, but also the elongation at break increased by the drawing. The toughness of the SBD nanocomposite (draw ratio = 3) was found to be 17 times higher than that of AC nanocomposite. Furthermore, the barrier properties of the nanocomposites remarkably increased due to the highly aligned MMT platelets. The SBD nanocomposite (draw ratio = 1.5) showed the excellent barrier properties similar to that of surface fluorinated PVA film. We believe that the orientation/alignment control of polymer/high-aspect-filler nanocomposites proposed in this study will contribute to develop a strategy for the fabrication of the high-performance polymer nanocomposites in a wide range of application in polymer composites science and engineering.

REFERENCES

1. A. Usuki, M. Kawasumi, Y. Kojima, Y. Fukushima, A. Okada, T. Kurauchi, O. Kamigaito, Swelling behavior of montmorillonite cation exchanged for ω-amino acids by ∈-caprolactam. *J. Mater., Res*., 8 (1993) 1174–1178.
2. A. Usuki, Y. Kojima, M. Kawasumi, A. Okada, Y. Fukushima, T. Kurauchi, O. Kamigaito, Synthesis of nylon 6-clay hybrid. *J. Mater., Res*., 8 (1993) 1179–1184.
3. Y. Kojima, A. Usuki, M. Kawasumi, A. Okada, Y. Fukushima, T. Karauchi, O. Kamigaito, Mechanical properties of nylon 6-clay hybrid. *J. Mater. Res.*, 8 (1993) 1185–1189.
4. Y. Kojima, A. Usuki, M. Kawasumi, A. Okada, Y. Fukushima, T. Karauchi, O. Kamigaito, Synthesis of nylon 6–clay hybrid by montmorillonite intercalated with ϵ-caprolactam. *J. Polym. Sci. Part A: Polym. Chem*., 31 (1993) 983–986.
5. Y. Kojima, A. Usuki, M. Kawasumi, A. Okada, Y. Fukushima, T. Karauchi, O. Kamigaito, One-pot synthesis of nylon 6–clay hybrid. *J. Polym. Sci. Part A: Polym*. *Chem*., 31 (1993) 1755–1758.
6. A. Okada, A. Usuki, Twenty Years of Polymer-Clay Nanocomposites. *Macromol. Mater. Eng.*, 291 (2006) 1449–1476.
7. M. Moniruzzaman, K. I. Winey, Polymer Nanocomposites Containing Carbon Nanotubes. *Macromolecules*, 39 (2006) 5194–5205.
8. D. R. Paul, L. M. Robeson, Polymer nanotechnology: Nanocomposites. *Polymer*, 49 (2008) 3187–3204.

9. H. Kim, A. A. Abdala, C. W. Macosko, Graphene/Polymer Nanocomposites. Macromolecules, 43 (2010) 6515–6530.

10. S. Morimune, M. Kotera, T. Nihino, K. Goto, K. Hata, Poly (vinyl alcohol) Nanocomposites with Nanodiamond. *Macromolecules*, 44 (2011) 4415–4421.

11. M. Morimune, T. Nishino, T. Goto, Poly (vinyl alcohol)/graphene oxide nanocomposites prepared by a simple eco-process. *Polym. J.*, 44 (2012) 1056–1063.

12. E. D. Laird, C. Y. Li, Structure and Morphology Control in Crystalline Polymer–Carbon Nanotube Nanocomposites. *Macromolecules,* 46 (2013) 2877–2891.

13. Y. Cui, S. I. Kundalwal, S. Kumar, Gas barrier performance of graphene/polymer nanocomposites. *Carbon*, 98 (2016) 313-333.

14. S. K. Kumar, B. C. Benicewicz, R. A. Vaia, K. I. Winey, 50th Anniversary Perspective: Are Polymer Nanocomposites Practical for Applications? *Macromolecules*, 50 (2017) 714–731.

15. S. Liu, S. Qin, Y. Jiang, P. Song, H. Wang, Lightweight high-performance carbon-polymer nanocomposites for electromagnetic interference shielding. *Compos. A: Appl. Sci. Manuf.*, 145 (2021) 106376.

16. S. Morimune, M. Kotera, T. Nishino, Stress transfer of poly (vinyl alcohol)/montmorillonite nanocomposite using X-ray diffraction. *J. Adh. Soc. Jpn.*, 46 (2010) 320–325.

17. D. García-López, J. F. Fernandez, J. C. Merino, J. Santarén, J. M. Pastor, Effect of organic modification of sepiolite for PA 6 polymer/organoclay nanocomposites. *Comp. Sci. Technol.*, 70

(2010) 1429-1436

18. Q. Fu, L. Medina, Y. Li, F. Carosio, A. Hajian, L. A. Berglund, Nanostructured Wood Hybrids for Fire-Retardancy Prepared by Clay Impregnation into the Cell Wall. *ACS Appl. Mater. Interfaces*, 9 (2017) 36154–36163.
19. C. Huang, Q. Cheng, Learning from nacre: Constructing polymer nanocomposites. *Comp. Sci. Technol.*, 150 (2017) 141-166.
20. T. T. Zhu, C. H. Zhou,F. B. Kabwe, Q. Q. Wu, C. S. Li, J. R. Zhang, Exfoliation of montmorillonite and related properties of clay/polymer nanocomposites. *Appl. Clay Sci.*, 169 (2019) 48-66.
21. X. Wan, Y. Qiao, Y. Zhang, Effect of different clay treatment on morphology and mechanical properties of PVC-clay nanocomposites. *Polym. Testing*, 22 (2003) 453–461.
22. B. Yalcin, M. Cakmak, The role of plasticizer on the exfoliation and dispersion and fracture behavior of clay particles in PVC matrix: a comprehensive morphological study. *Polymer*, 45 (2004) 6623–6638.
23. K. E. Strawhecker, E. Manias, Structure and Properties of Poly(vinyl alcohol)/Na+ Montmorillonite Nanocomposites. *Chem. Mater.*, 12 (2000) 2943–2949.
24. K. A. Carrado, P. Thiyagarajan, D. L. Elder, Polyvinyl Alcohol-Clay Complexes Formed by Direct Synthesis. *Clays Clay Mineral.*, 44 (1996) 506–514.
25. P. Podsiadlo, A. K. Kaushik, E. M Arruda, A. M. Waas, B. S. Shim, J. Xu, H. Nandivada, B. G.

Pumplin, J. Lahann, A. Ramamoorthy, N. A. Kotov, Ultrastrong and stiff layered polymer nanocomposites. *Science*, 318 (2007) 80–83.

26. R. A. Vaia, S. Vasudevan, W. Krawiec, L. G. Scanlon, E. P. Giannelis, New polymer electrolyte nanocomposites: Melt intercalation of poly(ethylene oxide) in mica-type silicates. *Adv. Mater.*, 7 (1995) 154–156.
27. S. Wong, R. A. Vaia, E. P. Giannelis, D. B. Zax, Dynamics in a poly(ethylene oxide)-based nanocomposite polymer electrolyte probed by solid state NMR. *Solid State Ionics*, 86 (1996) 547–557.
28. A. Liu, A. Walther, O. Ikkala, L. Belova, L. A. Berglund, Clay Nanopaper with Tough Cellulose Nanofiber Matrix for Fire Retardancy and Gas Barrier Functions. *Biomacromolecules*, 12 (2011) 633–641
29. J. J Kochumalayil, M. Bergenstråhle-Wohlert, S. Utsel, L. Wågberg, Q. Zhou, L. A Berglund, Bioinspired and Highly Oriented Clay Nanocomposites with a Xyloglucan Biopolymer Matrix: Extending the Range of Mechanical and Barrier Properties. *Biomacromolecules*, 14 (2013) 1, 84–91.
30. S. Morimune, M. Kotera, T. Nishino, Stress Transfer of Poly (vinyl alcohol) Montmorillonite Nanocomposites using X-ray Diffraction. *J. Adh. Soc. Jpn.*, 46 (2010) 320–325.
31. I. M. Ward, Mechanical properties of solid polymers, 2nd ed., John Wiley & Sons, New York, 1983, 246-328.

32. S. Morimune, M. Kotera, T. Nishino, T. Goto, Uniaxial Drawing of Poly (vinyl alcohol)/Graphene Oxide Nanocomposites. *Carbon*, 70 (2014) 38–45.

33. X. Pan, M. G. Debije, A. P. H. J. Schenning, C. W. M. Bastiaansen, Enhanced Thermal Conductivity in Oriented Polyvinyl Alcohol/Graphene Oxide Composites. *ACS Appl. Mater. Interfaces*, 13 (2021) 28864–28869

34. G. R. Gorrasi, D. Lieto, G. Patimo, S. D. Pasquale, A. Sorrentino, Structure–property relationships on uniaxially oriented carbon nanotube/polyethylene composites. *Polymer*, 52 (2011) 1124–1132.

35. P. Ciselli, R. Zhang, Z. Wang, C. T. Reynolds, M. Baxendale, T. Peijs, Oriented UHMW-PE/CNT composite tapes by a solution casting-drawing process using mixed-solvents. *Europ. Polym. J.*, 45 (2009) 2741–2748.

36. Y. Q. Rao, T. N. Blanton, Polymer Nanocomposites with a Low Thermal Expansion Coefficient. *Macromolecules*, 41 (2008) 935–941.

37. I. Sakurada, "*Polyvinyl Alcohol Fibers*," Marcel Dekker, Inc., New York, N.Y., 1985.

38. C.W. Bunn, Crystal Structure of Polyvinyl Alcohol. *Nature*, 161 (1948) 929.

39. K. Tashiro, H. Kitai, S. M. Saharin, A. Shimazu, T. Itou, Quantitative Crystal Structure Analysis of Poly(vinyl Alcohol)–Iodine Complexes on the Basis of 2D X-ray Diffraction, Raman Spectra, and Computer Simulation Techniques. *Macromolecules*, 48 (2015) 7, 2138–2148

40. K. Tashiro, K. Kusaka, H. Yamamoto, M. Hanesaka, Introduction of Disorder in Crystal Structures of Atactic Poly(vinyl Alcohol) and Its Iodine Complex To Solve a Dilemma between

X-ray and Neutron Diffraction Data Analysis. *Macromolecules*, 53 (2020) 6656-6671.

41. S. Huang, X. Cen, H. Peng, S. Guo, W. Wang, T. Liu, Heterogeneous Ultrathin Films of Poly(vinyl alcohol)/Layered Double Hydroxide and Montmorillonite Nanosheets via Layer-by-Layer Assembly. *J. Phys. Chem. B*, 113 (2009), 15225–15230.
42. A. Kato, S. Hamada, S. Shimizu, Study on microfracture mechanism of short glass fiber reinforcedpolycarbonate by using acoustic emission. *J. Appl. Polym. Sci.*, 135 (2018) 45664.
43. C. He, T. Liu, W. C. Tjiu, H. Sue, A. F. Yee, Microdeformation and Fracture Mechanisms in Polyamide-6/Organoclay Nanocomposites. *Macromolecules*, 41 (2008) 193–202.
44. K. Wang, L. Chen, J. Wu, M. L. Toh, C. He, A. F. Yee, Epoxy Nanocomposites with Highly Exfoliated Clay: Mechanical Properties and Fracture Mechanisms. *Macromolecules*, 38 (2005) 788–800.
45. R. A. Pearson, A. F. Yee, Toughening mechanisms in elastomer-modified epoxies. *J. Mater. Sci.*, 24 (1989) 2571–2580.
46. Y. Guo, Y. Xu, Q. Wang, Q. Dong, X. Yi, Y. Jia, Eliminating lightning strike damage to carbon fiber composite structures in Zone 2 of aircraft by Ni-coated carbon fiber nonwoven veils. *Comp. Sci. Technol.*, 169 (2019), 95–102.
47. Y. Nakamura, M. Yamaguchi, M. Okubo, T. Matsumoto, Effect of particle size on the fracture toughness of epoxy resin filled with spherical silica. *Polymer*, 33 (1992) 3415–3426.
48. G. M. Su, K. Best, T. Ranganathan, T. Emrick, A. J. Crosby, Tailored Nanoparticles for Enhancing

Polymer Adhesion. *Macromolecule*s, 44 (2011) 5256–5261.

49. H. Lu, Z. Chen, C. Ma, Bioinspired approaches for optimizing the strength and toughness of graphene-based polymer nanocomposites. *J. Mater. Chem.*, 32 (2012) 16182–16190.
50. M.-Y. Lim, H. J. Kim, S. J. Baek, K. Y. Kim, S.-S. Lee, J.-C. Lee, Improved strength and toughness of polyketone composites using extremely small amount of polyamide 6 grafted graphene oxides. *Carbon*, 77 (2014) 366–378.
51. T. Nishino, M. Meguro, K. Nakamae, Poly(vinyl alcohol) with Low Surface Free Energy by Fluorination. *Int. J. Adhes. Adhes.*, 19 (1999) 399–403.
52. B. Alexandrea, D. Langevina,P. Medericb, T. Aubryb, H. Couderca, Q. T. Nguyena, A. Saitera, S. Marais, Water barrier properties of polyamide 12/montmorillonite nanocomposite membranes: Structure and volume fraction effects. *J. Membrane Sci.*, 328 (2009) 186–204.
53. S. Nazarenko, P. Meneghetti, P. Julmon, B. G. Olson, S. Qutubuddin, Gas barrier of polystyrene montmorillonite clay nanocomposites: Effect of mineral layer aggregation. *J. Polym. Sci. Part B: Polym. Phys.*, 45 (2007) 1733–1753.